Impact of Training Strategies on Satellite-Based Solar Irradiance Forecast

Mariana B. Sousa, Rodrigo H. L. Farias, Alexandre C. A. Costa and Olga C. Vilela

Center for Renewable Energy (CER-UFPE), Federal University of Pernambuco (UFPE), Recife (Brazil)

Abstract

This article investigates the impact of training strategies on the performance of a satellite-based model with an artificial neural network (ANN) for solar irradiance forecasting. The methodology analyzes the influence of: (i) cyclic variables as model inputs; (ii) global horizontal irradiance (GHI) versus the clearness index (Kc) as target variables; (iii) ANN specialization for individual forecast horizons versus generalization across horizons; and (iv) hyperparameter optimization using the Optuna framework. The temporal analysis covers hourly forecasts from 1 to 9 hours ahead. The main findings indicate that using Kc as a target variable eliminates the need for cyclic input variables, compared to using GHI directly. This transition in feature dominance was also demonstrated: satellite PCs are dominant in horizons of up to 2 hours, while seasonal features become more prominent after 3 hours. The increase in complexity of the model did not translate linearly into accuracy gains. The generic ANN 9-MLP demonstrated the best cost-benefit ratio for the 1 hour-ahead horizon. However, for subsequent horizons, the 45 Specialized MLPs architecture presented the best overall error behavior and the best accuracy-cost trade-off. The analysis reinforces the nRMSE as the most reliable metric for performance comparison across different horizons.

Keywords: ANN, hourly, Kc, MLP, Optuna.

1. Introduction

Despite this growth, the intermittency and variability inherent in solar generation pose challenges to the stability and operation of the existing electrical infrastructure (REN21, 2023). In this scenario, solar irradiance and power forecasts are an indispensable tool for ensuring grid reliability and optimizing the management of solar assets.

When predicting solar irradiance, its cyclic pattern is the primary characteristic of modeling. The most well-known approach incorporates a clear-sky model (Yang, 2020; Chen et al., 2024). Furthermore, it is generally agreed that spatiotemporal variables (which capture cloud movement) improve forecasts by helping to capture the stochastic behavior of irradiance (Van der Meer et al., 2018; Chen et al., 2023).

The main forecasting methodologies focus on statistical models and numerical weather prediction models. Statistical models are frequently used for short-term forecasts (up to a few hours ahead), while numerical weather prediction models commonly exhibit better performance for longer forecast horizons (Verbois et al., 2023; Wen et al., 2023). Time series ground based models commonly outperform for intra-hourly horizons, due to the high correlation on the microphysics involved in this timescale, while numerical models take into account dynamic modelling of the atmosphere, cloud probability and then solar radiation transmissivity, so they outperform usually from 6h to several days ahead (Stefanov and Demsar, 2025). In this context, satellite-based models emerge as a robust and balanced solution for intra-day hourly forecasts (up to 4 to 6 hours ahead), filling the niche between ground-based and NWP approaches (e.g. Qin et al., 2022).

10.18086/swc.2025.04.27 Available at http://proceedings.ises.org

Machine learning (ML) tools are extensively employed in forecasting. Certain authors advocate specific ANN architectures as superior models, such as the Multi-Layer Perceptron (MLP) (e.g. Luo et al., 2021; Visser et al., 2022) or Long Short-Term Memory (LSTM) networks (e.g. Srivastava and Lessmann, 2018). Some researchers suggest that applying ML algorithms is more effective as a post-processing step than a standalone model (e.g. Yang et al., 2022). Others conclude that the selection of predictors and the optimization of hyperparameters are more critical than the choice of the model itself (e.g., Markovics and Mayer, 2022).

Many works in literature on solar forecasting have focused on benchmarking the performance of different model architectures, primarily on reporting the best accuracy achieved by each model on a given dataset (e.g., Azizi et al., 2023; Wen et al., 2023; Sebastianelli et al., 2024; Zang et al., 2024). Consequently, there is a gap in the literature for irradiance forecasts regarding the evaluation of the impacts of training strategies, such as feature engineering, target variable selection, and architecture optimization, which are crucial for model generalization and operational efficiency.

In an effort to synthesize and analyze some conclusions drawn from numerous studies, this paper proposes to take a specific model and train it through various approaches, by varying inputs, targets, and applying specialization and optimization of the ANN. Subsequently, the influence of these procedures on the model's performance was analyzed. The chosen model was satellite-based and utilizes a MLP algorithm, developed at the Center for Renewable Energy of the Federal University of Pernambuco (CER-UFPE) by Sabino (2019) with few modifications.

2. Methodology

This section outlines the steps used to achieve the forecast as the statistics to analyze and validate the model. The study was conducted in the cities of Petrolina, Águas Belas and Afogados, all located in the state of Pernambuco, Brazil (GMT-3).

2.1. Data Acquisition and Normalization

a) Satellite data

The satellite images used come from Channel 2 (Red Band) of the GOES-16 satellite and taken hourly (09:00,10:00, …, 20:00 - UTC). Due to the satellite's non-planar perspective, a reprojection to the reference coordinate system EPSG 4326 was applied. Subsequently, the spatial resolution was downsampled to 4 km x 4 km through bilinear interpolation. This reduction aims to reduce the input dimensionality, aligning the image granularity with the requirements of the prediction model. The final processing step resulted in the cropping of a fixed area of 131 x 131 pixels centered on the study station, defining the analysis region (as illustrated in Figure 1).

Figure 1: Cut of satellite images for each study location, Águas Belas, Afogados and Petrolina.

b) Ground Data

The data were obtained from the P&D project CHESF-Casa Nova (e.g. Petrolina) and from the Pernambuco solarimetric network (RedeSol-PE) (e.g., Afogados and Águas Belas).

The ground-based GHI measurements (minute resolution) were adjusted to a consistent hourly time step to match the satellite data. This was achieved through an integration process using the centered mean method, defined as the hourly mean between "hh:30" and "hh+1:29" and assigned the timestamp "hh+1:00". This methodology follows the approach detailed by Salazar et al. (2020). The resulting hourly GHI data served as the target variable for model training and subsequent validation. Crucially, no future data was used as input during either the training or prediction phases. Figure 2 shows raw data of each city in study. The days with no irradiance means that there weren't measurements. As the beginning of the year for Afogados e Belas Águas has a time mismatch, the date in this period was not considered for the training.

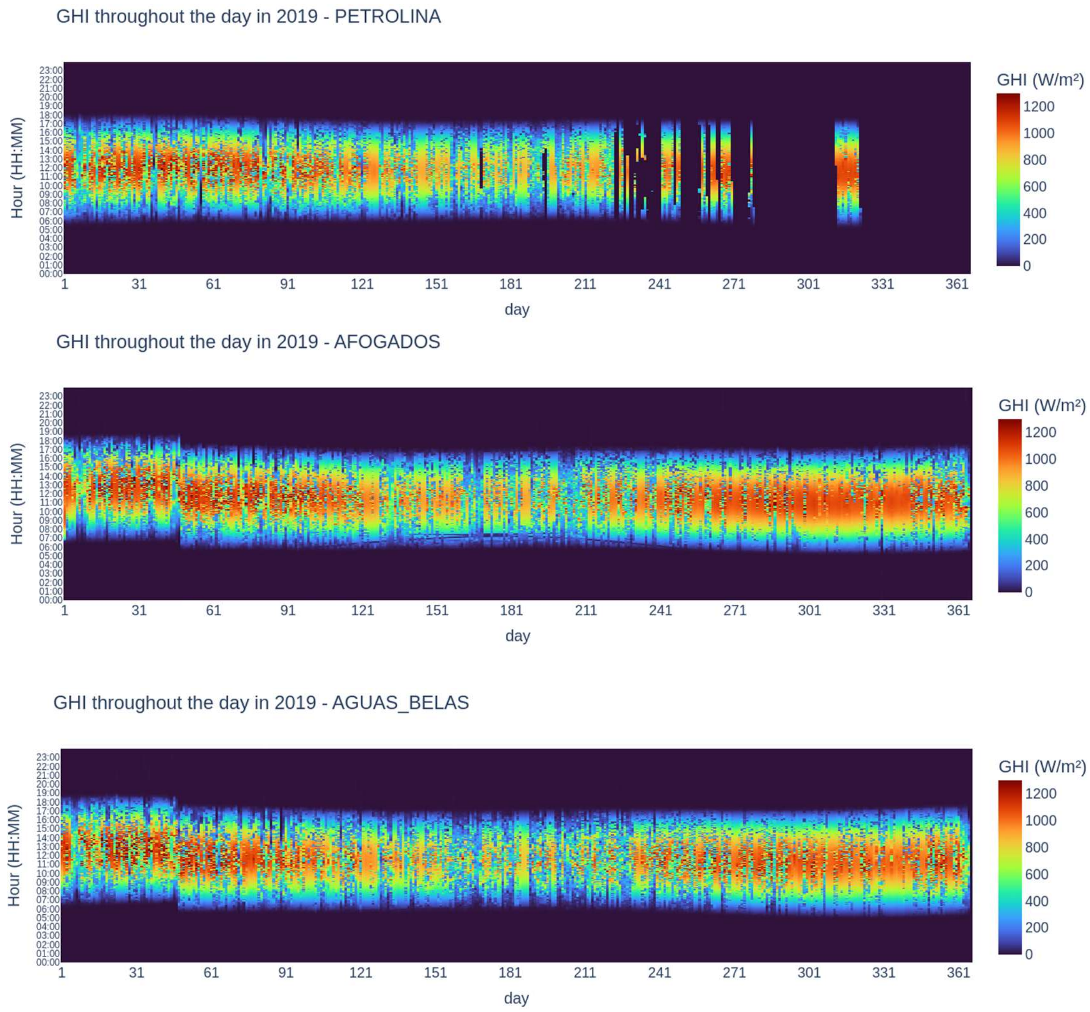

Figure 2: Irradiance throughout the day in 2019 for each study location, Aguas Belas, Afogados and Petrolina.

c) Clear-Sky Model

The clear-sky model employed was the McClear model provided by the Copernicus Atmosphere Monitoring Service (CAMS). This model was delivered with high temporal resolution (1min) and went through the same integration procedure as the measured data. This model was used to determine the clear-sky index (Kc) (eq. 1). Kc was employed as an alternative to GHI as the target in the model and to compare the results. Here is a difference with the original model that forecasts only GHI.

$$K_c = GHI_{measured} / GHI_{ClearSky} \quad \text{(eq. 1)}$$

2.2. Irradiance Map Generation

a) Clear and Cloud Index Calculation

The Clear Index (L_{clr}) and a Cloud Index (L_{cld}) calculated for each pixel is based on the Brasil-SR model

(Martins et al., 2004). L_{clr} and L_{cld} were defined as the lowest and highest pixel brightness value observed over the preceding 30 images for a determined pixel at a determined hour.

This approach differs significantly from Sabino's (2019) reference model. The previous work required a full year of data to determine these indices (fixed for each hour of the month) at a stationary stage, thus requiring a second distinct year of imagery exclusively for model training. The new methodology requires only one year of data in the training phase, using the adaptive sliding window of the most recent 30 days to continuously and dynamically infer these indices at the time of map creation. This optimization drastically reduces storage requirements and the time for dataset acquisition and preprocessing.

b) Transmittance Parametrization

The minimum (Kt_{min}) and maximum (Kt_{max}) atmospheric transmittance (k_t) values were calculated using GHI data from the year of the training period. To this end, the basic astronomical and cyclical variables — Minute of the Year (MoY) (eq. 2); Angle of the Year (MoY_{Angle}) (eq. 3); Eccentricity Factor ($E0$) (eq. 4), developed by Spencer (Miguel et al., 2021); and Extraterrestrial Irradiation (I_0) (eq. 5) — were determined to calculate k_t series (eq. 6). Then Kt_{min} and Kt_{max} were defined for each hour of each month.

$$MoY = (Day - 1) * 60 + hours * 60 + minutes \quad \text{(eq. 2)}$$

$$MoY_{Angle} = (2 * \pi * MoY) \div (365 * 24 * 60) \quad \text{(eq. 3)}$$

$$E0 = 1.00011 + 0.034221 * cos(MoY_{Angle}) + 0.001280 * sin(MoY_{Angle}) + 0.000719 * cos(2 * MoY_{Angle}) + 0.000077 * sin(2 * MoY_{Angle}) \quad \text{(eq. 4)}$$

$$I_0 = 1367 * E0 \quad \text{(eq. 5)}$$

$$k_t = \frac{GHI_{medido}}{I_0 * cos(zenithal\ angle)} \quad \text{(eq. 6)}$$

c) GHI Calculation

The Cloud Cover Index (CCI) was calculated for each pixel (eq. 7). Subsequently, GHI for each pixel was determined by eq. 8.

$$CCI = (pixel_{brightnes} - L_{clr})/(L_{clr} - L_{cld}) \quad \text{(eq. 7)}$$

$$GHI = I_0 * cos(zenithal\ angle) * [(Kt_{max} - Kt_{min}) * (1 - CCI) + Kt_{min}] \quad \text{(eq. 8)}$$

2.3. Feature Engineering and Model Input

a) Feature Selection and Dimensionality Reduction

Initially, the correlation between the $GHI_{measured}$ at the ground station and the GHI values of each satellite pixel was calculated. Then, the correlation was temporally shifted (t_{-k}) by the forecast horizon of interest from the ground data. The 10% of pixels with the highest absolute correlation (either positively or inversely correlated) were selected. To manage the resulting large number of inputs (1716 pixels), Principal Component Analysis (PCA) was applied, and the 8 most relevant components were selected for each irradiance map (or image), following the original methodology.

b) Cyclic and Temporal Variables

In addition to the principal components (PC), 8 cyclic variables utilizing fuzzy logic (0 to 1) were created to capture the temporal patterns of solar irradiance: 4 representing the four seasons (spring, summer, fall, and winter); and 4 representing the diurnal cycle, as depicted in Figure 3. The nighttime (18h to 5h local time) was disregarded, but just for representation they are in the graphs.

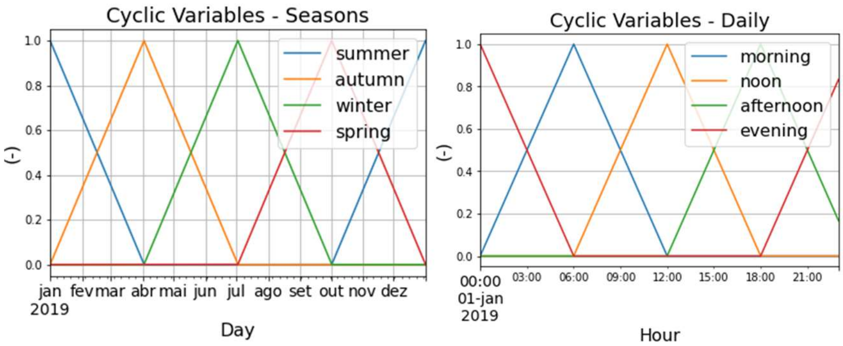

Figure 3: Cyclical variables for input into the model. On the left, the four seasonal variables. On the right, the four daily variables.

2.4. Prediction Model and Evaluation

a) Artificial Neural Network (ANN) Configuration

The forecasting tool employed the Multilayer Perceptron (MLP) architecture. The inputs to the MLPs were:

- The 8 principal components extracted from each of the three most recent images (t , t_{-1} and t_{-2}).
- The 8 cyclic variables correspond to the desired target time (t_{+k}).

The primary target of the model was the hourly GHI measurement. Additionally, the clear-sky model was converted into K_c and used as an alternative target for comparative analysis. When K_c was the target, an additional step to convert it to GHI was applied, by manipulating eq. 1, at the end of the process and then evaluated.

Two main MLP configurations were tested:

- One MLP per forecast horizon: A total of 9 MLPs were trained (horizons from 1 to 9 hours ahead).
- One MLP per forecast horizon for each launch time: This resulted in 45 MLPs (one for each forecast horizon, 1 to 9 hours ahead, for each launch time 8:00 to 16:00).

To evaluate the impact of hyperparameter optimization, the study was conducted in two distinct phases. Initially, a baseline model was established with fixed hyperparameters: two hidden layers with 5 and 8 neurons, respectively, using the ReLU activation function, an initial pseudorandomness seed of 0 and batch size of 10, aiming at reproducibility. In the second phase (called "Optimized"), the Optuna optimization framework was incorporated to search for the optimal MLP configuration and analyze its impact on performance.

The search space in the second phase was purposefully restricted to 200 configuration trials, aiming to maintain computational efficiency and mitigate the risk of overfitting. The degrees of freedom defined were: the number of hidden layers (between 1 and 3); the number of neurons per layer (between 1 and 10); and the ReLU or Sigmoid activation functions. The restriction on the number of neurons was a deliberate decision to optimize cost-benefit and avoid excessive complexity, given the feature set already reduced by PCA. Finally, the optimal configuration determined by Optuna was subjected to a robust analysis: the model was retrained 100 times using different initialization seeds. The final model, selected for results analysis, was the one that demonstrated the lowest Root Mean Squared Error (RMSE) among the 100 runs, ensuring the selection of the most efficient initialization and increasing confidence in the generalization of the results. The dataset to train with the optimization tool was split into 70% for training and 30% for validation.

b) Reference model

For solar forecasts, the reference model is called Smart Persistence (Chen et al., 2024) (eq. 9). This model takes account of the cyclic pattern of solar radiation through a clear-sky model. Here, the Mc Clear Model as the clear-sky was used.

$$GHI_{t+k} = \frac{GHI_t}{GHI_{ClearSky,(t)}} * GHI_{ClearSky,(t+k)} \quad \text{(eq. 9)}$$

c) Performance Metrics

The statistical metrics utilized to evaluate the forecast performance were the Root Mean Squared Error (RMSE) (eq. 10), normalized RMSE (eq. 11) and Pearson's correlation coefficient (r) (eq. 12).

$$RMSE = \sqrt{\frac{\sum_i^n (predicted_i - actual_i)^2}{n}} \quad \text{(eq. 10)}$$

$$nRMSE = \frac{RMSE}{mean} \quad \text{(eq. 11)}$$

$$r = \frac{Cov(predicted, actual)}{\sigma_{predicted}\sigma_{actual}} \quad \text{(eq. 12)}$$

3. Results

As depicted in Figure 4 (a, b and c), Principal Components (PC) derived from satellite imagery constituted the primary input variables up to 2 hours ahead (red line) when GHI was the target of the model. Beyond this horizon, the cyclic patterns (green curve) became the dominant relevant features. This finding aligns with the established understanding that time series models perform effectively over shorter durations due to the high autocorrelation observed in short-term periods, after which the seasonal behavior becomes more influential. However, when Kc is used as the target variable instead, utilizing only PC features from satellite imagery proves sufficient, and the cyclic variables are no longer necessary. The Kc target seems to incorporate inherently the deterministic cyclic pattern. The observed pattern of decreasing error with increasing forecast horizons might initially seem counterintuitive. However, this behavior can be attributed to the specialization of the ANNs towards the target times. As the forecast horizon extends, the target time shifts towards the end of the day, when solar irradiance is typically lower, thus leading to lower absolute errors. Despite this decrease in error, the nRMSE consistently increases, reinforcing the robustness of the results.

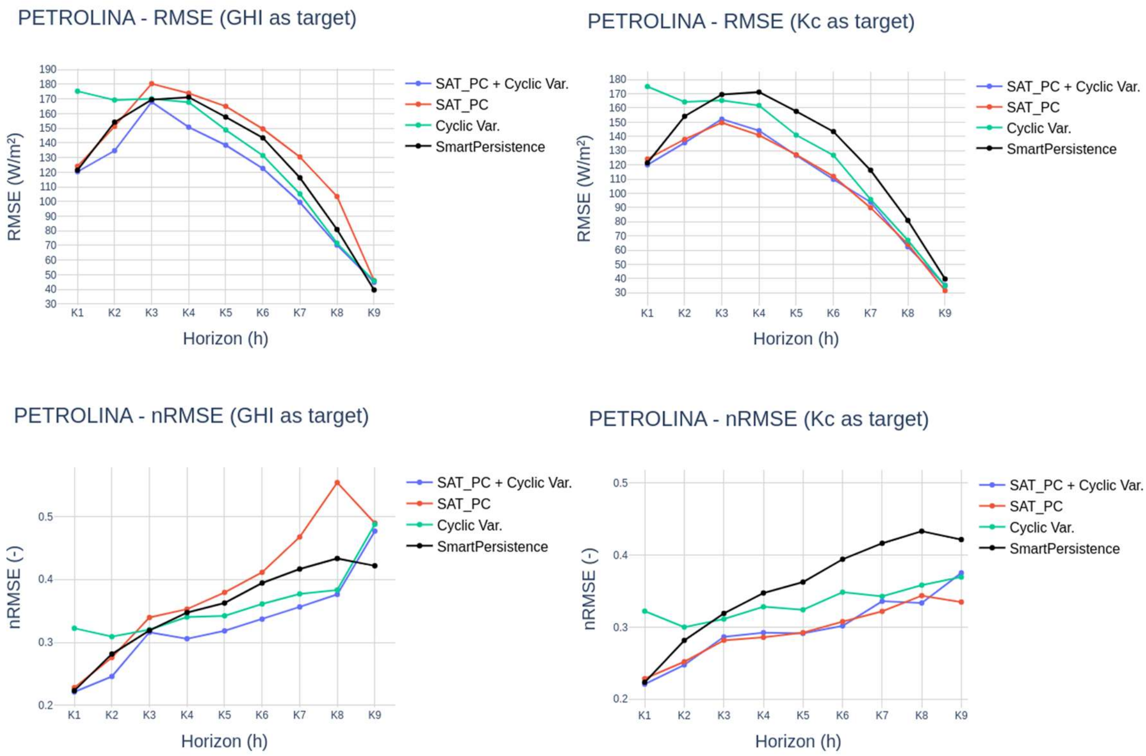
PETROLINA - RMSE (GHI as target)
RMSE (W/m²)
Horizon (h)
SAT_PC + Cyclic Var.
SAT_PC
Cyclic Var.
SmartPersistence
PETROLINA - RMSE (Kc as target)
RMSE (W/m²)
Horizon (h)
SAT_PC + Cyclic Var.
SAT_PC
Cyclic Var.
SmartPersistence
PETROLINA - nRMSE (GHI as target)
nRMSE (-)
Horizon (h)
SAT_PC + Cyclic Var.
SAT_PC
Cyclic Var.
SmartPersistence
PETROLINA - nRMSE (Kc as target)
nRMSE (-)
Horizon (h)
SAT_PC + Cyclic Var.
SAT_PC
Cyclic Var.
SmartPersistence

(a)

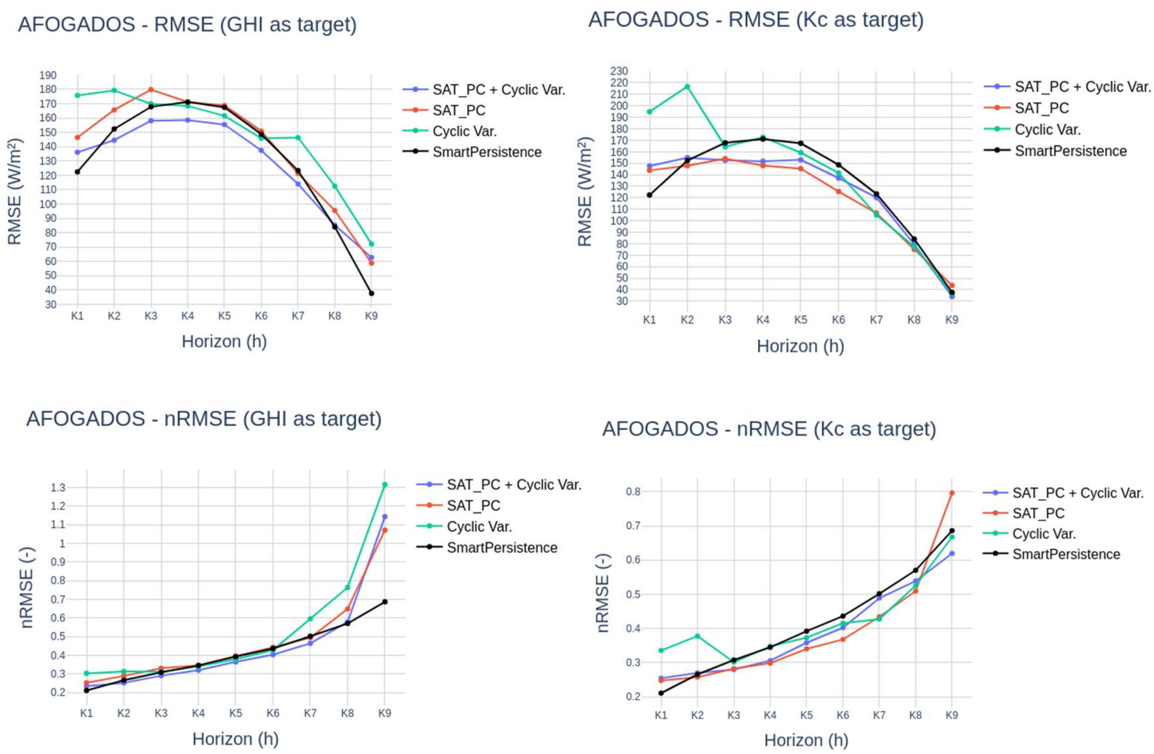
AFOGADOS - RMSE (GHI as target)
RMSE (W/m²)
Horizon (h)
SAT_PC + Cyclic Var.
SAT_PC
Cyclic Var.
SmartPersistence
AFOGADOS - RMSE (Kc as target)
RMSE (W/m²)
Horizon (h)
SAT_PC + Cyclic Var.
SAT_PC
Cyclic Var.
SmartPersistence
AFOGADOS - nRMSE (GHI as target)
nRMSE (-)
Horizon (h)
SAT_PC + Cyclic Var.
SAT_PC
Cyclic Var.
SmartPersistence
AFOGADOS - nRMSE (Kc as target)
nRMSE (-)
Horizon (h)
SAT_PC + Cyclic Var.
SAT_PC
Cyclic Var.
SmartPersistence

(b)

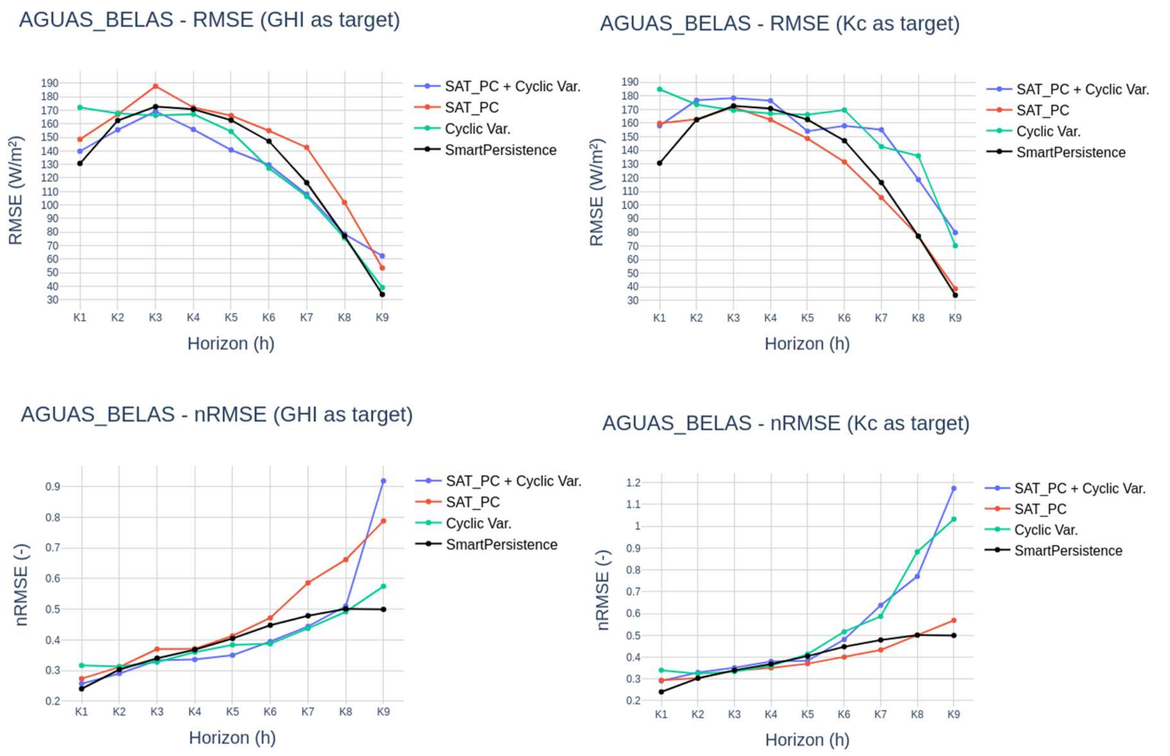

(c)

Figure 4: RMSE and nRMSE of the model according to the input variables. (a) Petrolina; (b) Afogados; (c) Águas Belas.

The statistical analysis presented in Figure 5 (a, b, and c) was conducted using exclusively the Principal Component (PCs) derived from the satellite images, since these produced the best results with Kc as the target in the previous step. The results compare four modeling approaches: a) Simple (Baseline - Red Line), b) Specialized (Green Line), c) Optimized Optuna (Blue Line), and d) 45 Specialized MLPs (Orange Line).

For the shorter horizon (1 hour ahead), it is observed that increasing the complexity of the architecture does not result in consistent performance improvement. The Specialized (Green Line) and Optimized (Blue and Orange Lines) approaches had difficulty outperforming the Simple approach (Baseline - Red Line). There was a maximum reduction of 2% in RMSE only in the Afogados case study, with no significant gains in Petrolina and Águas Belas. This initial result suggests that, for immediate forecasts, the high complexity introduced does not translate into superior accuracy.

In subsequent forecast horizons, the set of 45 Specialized MLPs (Orange Line) demonstrated the best overall error behavior and the best cost-benefit ratio (precision-cost trade-off) in the three locations studied. Although this approach shows marginally inferior performance in the worst case (Águas Belas, 1 hour ahead), with a 6% difference compared to the best approach, its training cost is relatively low (Table 1). Only in the case of Petrolina did the more complex approach (Optimized Optuna or 45 MLPs) lead to the lowest errors, with a 2% gain in RMSE, compensated, however, by a higher training cost (almost 4 hours, Table 1).

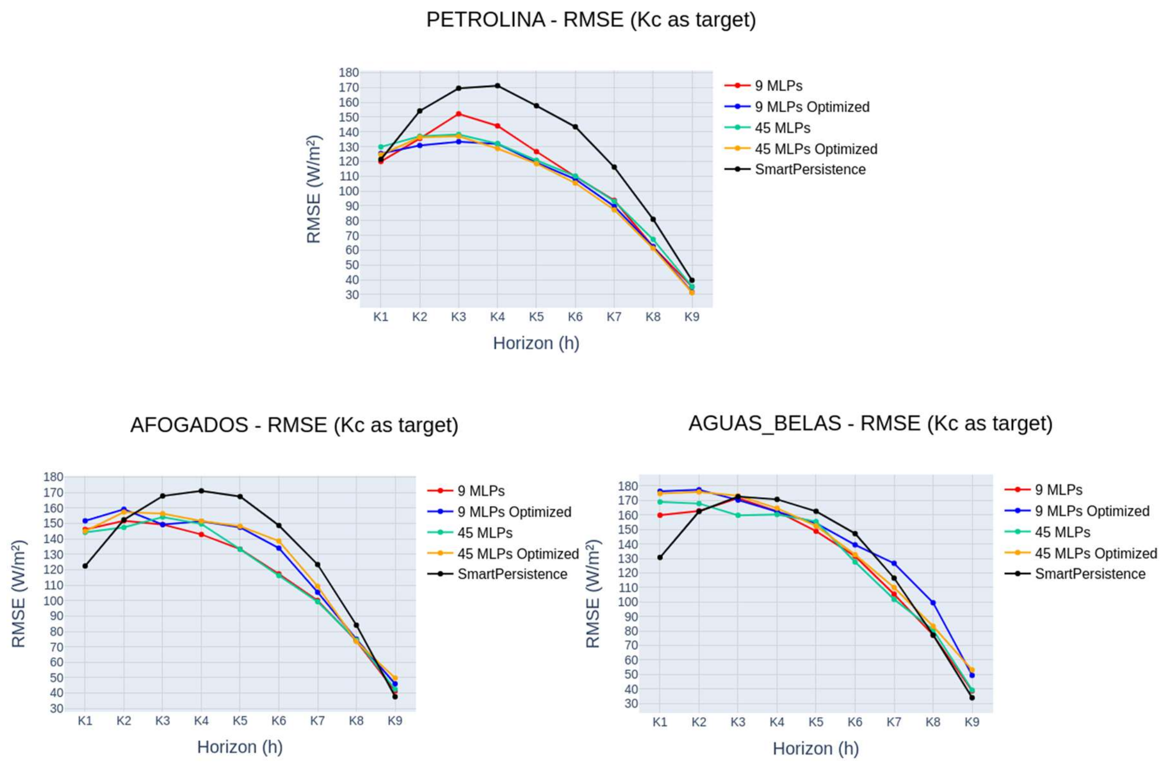
PETROLINA - RMSE (Kc as target)
AFOGADOS - RMSE (Kc as target)
AGUAS_BELAS - RMSE (Kc as target)
RMSE (W/m²)
Horizon (h)
K1 K2 K3 K4 K5 K6 K7 K8 K9
9 MLPs
9 MLPs Optimized
45 MLPs
45 MLPs Optimized
SmartPersistence

(a)

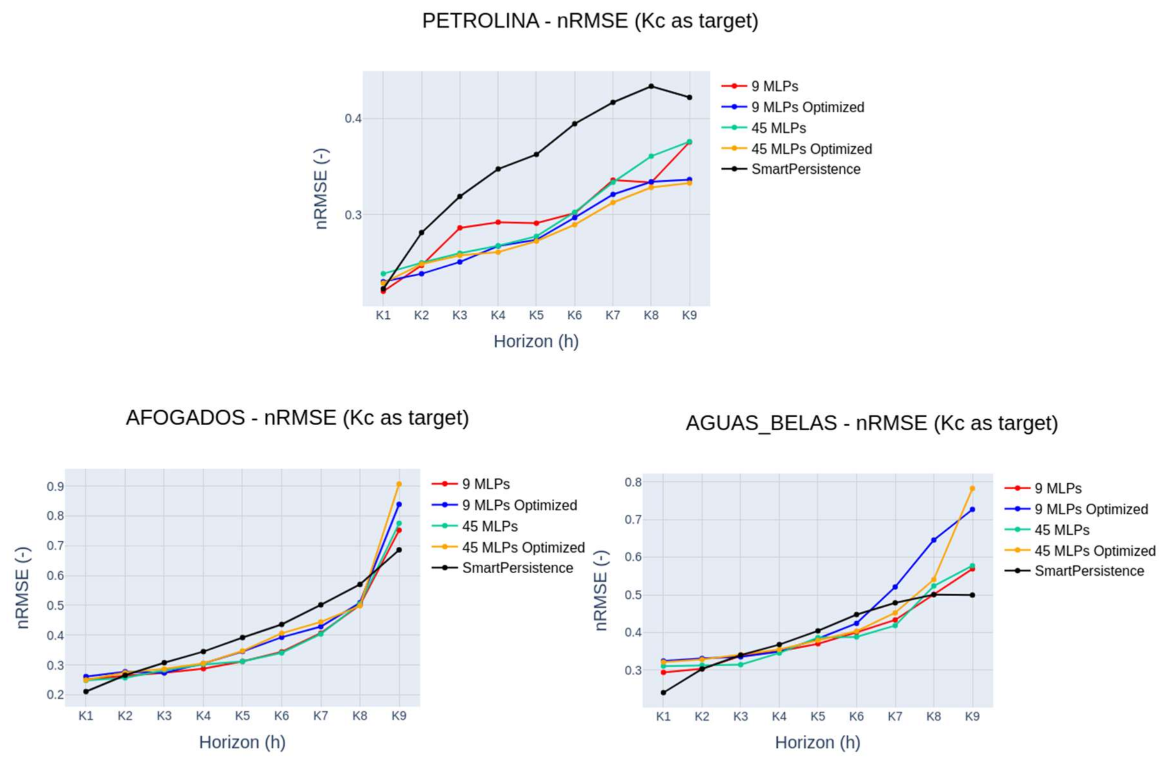
PETROLINA - nRMSE (Kc as target)
AFOGADOS - nRMSE (Kc as target)
AGUAS_BELAS - nRMSE (Kc as target)
nRMSE (-)
Horizon (h)
K1 K2 K3 K4 K5 K6 K7 K8 K9
9 MLPs
9 MLPs Optimized
45 MLPs
45 MLPs Optimized
SmartPersistence

(b)

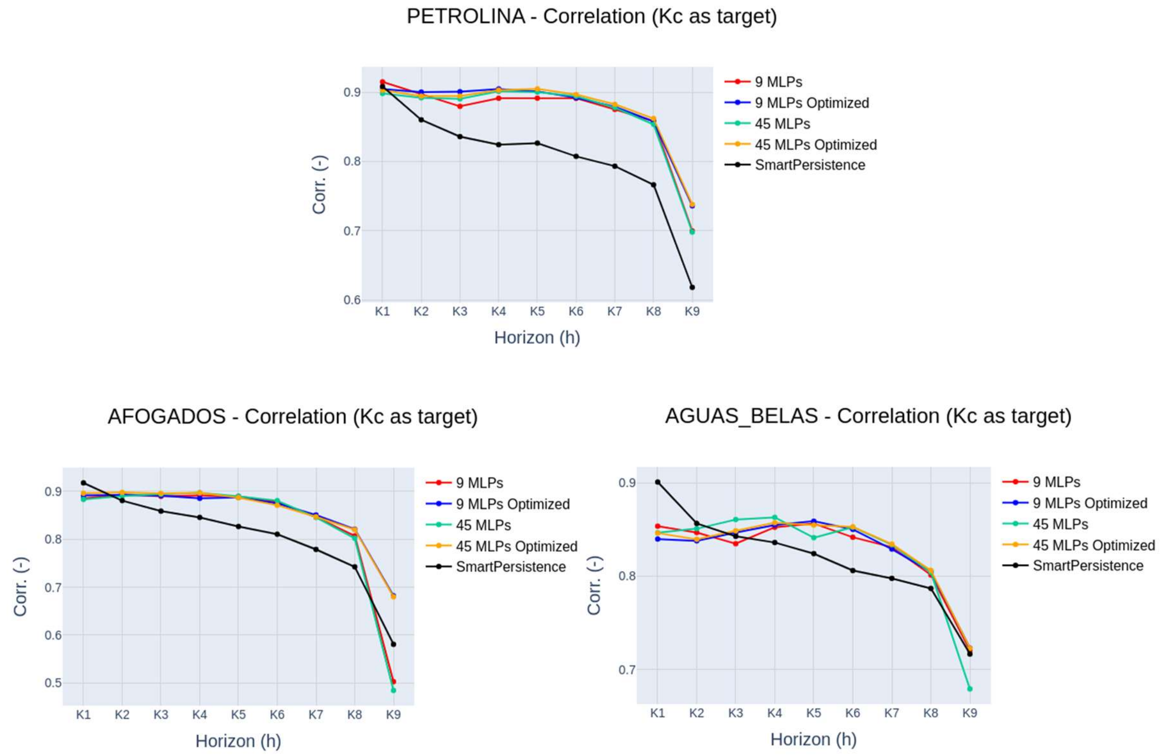

(c)

Figure 5: Statistics for evaluating architecture and optimization. (a) RMSE; (b) nRMSE; (c) Correlation.

Table 1: Table of training time duration.

Configuration	Training Duration
9 MLPs	~ 2 minutes
9 MLPs with optimization	~ 32 minutes
45 MLPs	~ 8 minutes
45 MLPs with optimization	~ 3h and 44 minutes

4. Conclusions

The results of this research provide relevant insights into feature engineering and ANN optimization for solar irradiance forecasts. The conclusions that can be drawn from this work, considering the main findings, scientific implications, and recommendations for future work, are:

Main findings

1. Enhancement via Kc and Feature Engineering Simplification: Using the Clearness Index Kc as a target variable proved to be the most effective strategy. By intrinsically incorporating the deterministic component of solar irradiance, Kc simplified modeling, making conventional seasonality features unnecessary. This allowed the model to operate exclusively with the Principal Components derived from the satellite, maintaining or exceeding the performance of models that use GHI directly.
2. Feature Dominance Transition: The dominance transition of the input variables as a function of the forecast horizon was clearly demonstrated. For horizons up to 2 hours, satellite PCs are dominant, reflecting the high autocorrelation of the time series in the short term. However, from 3 hours onwards, seasonal and deterministic features become more prominent (when GHI is the target).
3. Architecture Optimization and Cost-Benefit: The complexity of the model does not translate linearly into accuracy gains. The generic 9 MLP architecture demonstrated the best cost-benefit ratio

(precision-cost trade-off) for the 1 hour-ahead horizon. However, for subsequent forecast horizons, the 45 MLPs architecture without hyperparameter optimization showed the best overall error behavior. This approach has a low training cost (approximately 8 minutes, Table1) while maintaining consistently low error beyond 1 hour.

Implications

- Investigation of the Applicability of Operational Clear Sky Models: Although the McClear model is not inherently operational, the success of the Kc variable demonstrates the potential of the approach. It is suggested that future research investigate and compare the performance of operational clear sky models (using real-time data) within the forecasting framework. This analysis should take into account location dependence and climate regime, as the accuracy of deterministic component separation varies significantly across different geographic regions.
- Design Guideline for Computational Efficiency: The main implication is the need to focus on efficiency, favoring the optimization of simpler and more robust architectures or the development of more specialized architectures that dispense with complex optimization tools. This finding establishes a clear guideline for model design, prioritizing operational cost-effectiveness over fractional RMSE gain.

Recommendations for Future Work

- Analysis of clear-sky models in forecast: Although the McClear model is not inherently operational, the success of the Kc variable demonstrates the potential of the approach. It is suggested that future research investigate and compare the performance of operational clear-sky models (using real-time data) within the forecasting framework. This analysis should take into account location dependence and weather regime, as the accuracy of deterministic component separation varies significantly across different geographic regions.
- Exhaustive Comparison of Kc and GHI: It is recommended that future studies focus on a direct, systematic, and multi-location comparison of the performance of models trained with the Kc versus GHI as target variables. The primary objective of this exhaustive validation is the isolation and rigorous quantification of the accuracy gain or simplification as a function of the selected target variable under different climatological conditions and datasets.

5. Acknowledgements

This work received fundamental support from the ZeroC-PE Network (Research, Development, and Innovation Network for Green Hydrogen and Zero-Emission Technologies of Pernambuco) - FACEPE.

Additionally, we are grateful to the São Francisco Hydroelectric Company (CHESF-ELETROBRAS) for their support through the CHESF-CASANOVA project, ANEEL CODE: PD-00048-0217.

6. References

Azizi, N. et al, 2023. Deep learning based long-term global solar irradiance and temperature forecasting using time series with multi-step multivariate output. Renewable Energy, v. 206, p. 135–147.

Chen, S. et al, 2023. Global and direct solar irradiance estimation using deep learning and selected spectral satellite images. Applied Energy. v. 352.

Chen, S. et al, 2024. Improved satellite-based intra-day solar forecasting with a chain of deep learning models. Energy Conversion and Management, v. 313, p. 118598, ago.

Luo, X.; Zhang, D.; Zhu, X., 2021. Deep learning based forecasting of photovoltaic power generation by incorporating domain knowledge. Energy, v. 225, p. 120240.

Markovics, D.; Mayer, M. J., 2022. Comparison of machine learning methods for photovoltaic power forecasting based on numerical weather prediction. Renewable and Sustainable Energy Reviews, v. 161, p. 112364.

Martins, F.R.; Pereira, E. B.; Echer, M. P. d. S., 2004. Levantamento dos recursos de energia solar no Brasil com o emprego de satélite geoestacionário: o Projeto Swera. Revista Brasileira de Ensino de Física, v. 26, n. 2, p. 145–159.

Miguel, H. et al, 2021. Estimation of daily energy gain of solar tracking surfaces based on geographic position. Revista Ifes Ciência, v. 7, n. 1, p. 01-14.

Qin, J. et al, 2022. Enhancing solar PV output forecast by integrating ground and satellite observations with deep learning. Renewable and Sustainable Energy Reviews, v. 167, p. 112680.

REN21, 2023. Renewable energy policy network for the 21st century. Renewables global status report. Paris.

Salazar, G. et al, 2020. Solar irradiance time series derived from high-quality measurements, satellite-based models, and reanalyses at a near-equatorial site in Brazil. Renewable and Sustainable Energy Reviews, v. 117, p. 109478.

Sabino, Edson Ricardo Calado, 2019. Previsão de radiação solar e temperatura ambiente voltada para auxiliar a operação de usinas fotovoltaicas.

Sebastianelli, A. et al, 2024. Machine learning forecast of surface solar irradiance from meteo satellite data. Remote Sensing of Environment, v. 315, p. 114431–114431.

Stefanov, D; Demsar, J, 2025. Forecasting solar power production by using satellite images. Solar Energy, v. 300, p. 113823.

Srivastava, S.; Lessmann, S., 2018. A comparative study of LSTM neural networks in forecasting day-ahead global horizontal irradiance with satellite data. Solar Energy, v. 162, p. 232–247.

Van Der Meer, D. W.; Widén, J.; Munkhammar, J., 2018. Review on probabilistic forecasting of photovoltaic power production and electricity consumption. Renewable and Sustainable Energy Reviews, v. 81, p. 1484–1512.

Verbois, H. et al, 2023. Improvement of satellite-derived surface solar irradiance estimations using spatio-temporal extrapolation with statistical learning. Solar Energy, v. 258, p. 175–193.

Visser, L.; Alskaif, T.; Van Sark, W., 2022. Operational day-ahead solar power forecasting for aggregated PV systems with a varying spatial distribution. Renewable Energy, v. 183, p. 267–282.

Wen, H. et al. A regional solar forecasting approach using generative adversarial networks with solar irradiance maps. Renewable Energy, v. 216, p. 119043.

Yang, D., 2020. Choice of clear-sky model in solar forecasting. Journal of Renewable and Sustainable Energy, v. 12, n. 2, p. 026101.

Yang, D. et al, 2022. A Concise Overview on Solar Resource Assessment and Forecasting. Advances in Atmospheric Sciences, v. 39, n. 8, p. 1239–1251.

Zang, H. et al, 2024. Multi-site solar irradiance forecasting based on adaptive spatiotemporal graph convolutional network. Expert Systems with Applications, v. 236, p. 121313–121313.